Analysis of natural variants of the hepatitis C virus internal ribosome entry site reveals that primary sequence plays a key role on cap-independent translation

María Inés Barría[1,2], Angel González[3], Jorge Vera-Otarola[1,2], Ursula León[1,2], Valeska Vollrath[1,2], Delphine Marsac[1,2], Octavio Monasterio[4], Tomás Pérez-Acle[3,5], Alejandro Soza[2,6] and Marcelo López-Lastra[1,2,*]

[1]Laboratorio de Virología Molecular, Centro de Investigaciones Médicas, Facultad de Medicina, Pontificia Universidad Católica de Chile, [2]Jeunes Equipes Associées à l'IRD y Nucleo Milenio de Inmunología e Inmunoterapia, [3]Centre for Bioinformatics (CBUC), Facultad de Ciencias Biológicas, Pontificia Universidad Católica de Chile, [4]Departamento de Biología, Facultad de Ciencias, Universidad de Chile, [5]Fundación Ciencia para la Vida and [6]Departamento de Gastroenterología, Facultad de Medicina, Pontificia Universidad Católica de Chile, Santiago, Chile

ABSTRACT

The HCV internal ribosome entry site (IRES) spans a region of ~340 nt that encompasses most of the 5′ untranslated region (5′UTR) of the viral mRNA and the first 24–40 nt of the core-coding region. To investigate the implication of altering the primary sequence of the 5′UTR on IRES activity, naturally occurring variants of the 5′UTR were isolated from clinical samples and analyzed. The impact of the identified mutations on translation was evaluated in the context of RLuc/FLuc bicistronic RNAs. Results show that depending on their location within the RNA structure, these naturally occurring mutations cause a range of effects on IRES activity. However, mutations within subdomain IIId hinder HCV IRES-mediated translation. In an attempt to explain these data, the dynamic behavior of the subdomain IIId was analyzed by means of molecular dynamics (MD) simulations. Despite the loss of function, MD simulations predicted that mutant G266A/G268U possesses a structure similar to the wt-RNA. This prediction was validated by analyzing the secondary structure of the isolated IIId RNAs by circular dichroism spectroscopy in the presence or absence of Mg^{2+} ions. These data strongly suggest that the primary sequence of subdomain IIId plays a key role in HCV IRES-mediated translation.

INTRODUCTION

Translation initiation of the vast majority of eukaryotic mRNAs occurs by a scanning mechanism, whereby the recognition of the mRNA's 5′cap structure (m^7GpppN) by eukaryotic translation initiation factors (eIFs) is followed by the binding of the 40S ribosomal subunit and scanning downstream to the initiation codon (1,2). The initiation factor eIF4F is responsible for positioning the 40S ribosomal subunit in proximity to the 5′cap structure. The 40S subunit is recruited to the mRNA as part of the 43S initiation complex, composed of the subunit bound to eIF2-GTP/Met-tRNAi (ternary complex), eIF1, eIF1A and eIF3. Upon attachment to the vicinity of the cap the ribosomal subunit scans the mRNA in a 5′ to 3′ direction until the initiation codon is encountered leading to the formation of the 48S initiation complex in which the initiator AUG is base paired to the anticodon of the initiator tRNA. At this stage, the eIFs are displaced from the 40S ribosomal subunit allowing the joining of the 60S subunit. Ribosomal subunit joining results in the formation of an 80S ribosome in which the initiator Met-tRNA is positioned in the ribosomal peptidyl (P) site (3,4). In contrast to the canonical mechanism of eukaryotic translation initiation, the hepatitis C virus (HCV) mRNA uses an alternative ribosome recruitment mechanism by which the 40S ribosomal subunits directly binds to an RNA structure termed the HCV-internal ribosome entry site (IRES) (5–7). Ribosomal subunit binding to the HCV-IRES occurs in the absence of eIFs, in such a way that

the initiation codon is placed in the immediate vicinity of the ribosomal P site not requiring ribosomal scanning (5,8,9). Subsequent addition of the ternary complex to the 40S/IRES complex is necessary and sufficient for the formation of the 48S complexes (5,6,8). Translation initiation factor eIF3 is not needed for 48S complex formation (10), however it specifically binds to the HCV IRES and is required for subsequent joining of the 60S subunit to the 48S complex to form functional 80S ribosomes (5).

The HCV IRES spans a region of $\sim$340 nt that encompasses most of the 5′ untranslated region (UTR) of the viral mRNA and the first 24–40 nt of the core coding region (11,12). Under a physiological concentration of magnesium ions and in the absence of any additional factor, the 5′UTR is predicted to fold into a complex secondary/tertiary structure characterized by four major domains designated I to IV (13). Domains II, III and IV are necessary for IRES activity (14). Domain III is required for 40S ribosomal subunit and eIF3 binding (7,10,15,16). Domain II is responsible for the substantial conformational changes in 40S subunits induced by IRES binding (7), and for efficient eIF5-induced hydrolysis of eIF2-bound GTP in the 48S complexes assembled on the IRES (17). Domain IV contains the initiation codon and a portion of the Core protein open reading frame (ORF) (18).

Mutational analysis of the HCV IRES shows that the integrity of the higher order RNA structure is critical for HCV IRES activity (19–21). In an effort to further characterize the function of the different IRES structural domains on IRES function we undertook the challenge of identifying naturally occurring mutations within the HCV IRES of viral species present in clinical samples and evaluated their effect on translation in the context of a bicistronic RNA. In this study the 1b-IRES recovered from the HCV replicon pFK-I$_{377}$neo/NS3-3′/wt was used as the wild-type (wt) IRES (22). Sequence analysis revealed that different isolates displayed diverse sets of mutations. The role of the each natural variant in IRES function was evaluated by introducing independent or combined mutations within the sequence of the wt 1b-IRES. Our results show that depending on their location within the RNA structure, mutations cause a range of effects on IRES activity. Notably and in agreement with previous reports, we find that mutations within the IRES IIId subdomain have the most drastic effects on HCV IRES activity. In an attempt to further explain these observations, the dynamic behavior of the reference wt-IRES and of the specific mutations within the IRES subdomain IIId was analyzed by means of molecular dynamics (MD) simulations. Strikingly, MD analysis predicted that one of the isolated mutants in the IIId subdomain, namely mutant G266A/G268U, exhibited structural conservation with respect to the wt-IRES. This prediction was confirmed by circular dichroism (CD) spectroscopy. Together, our results confirm the stringent structure/function relationship exhibited by the HCV IRES, but also suggest that the primary sequence of subdomain IIId plays a role in, and is required, for IRES-mediated translation initiation.

MATERIALS AND METHODS

Patients

Nineteen patients recruited from the outpatient clinic of the Hepatology Unit of the Clinical Hospital, Pontificia Universidad Católica de Chile (PUC) were included in this study. Protocols followed in this study were approved by the Ethical Review Board of the Faculty of Medicine, PUC. Donors signed a written consent form also approved by the Ethical Review Board of the Faculty of Medicine, PUC, before donating blood. Patient inclusion criteria have been described elsewhere (23). All patients were naïve to antiviral treatment. Both plasma and peripheral blood mononuclear cells (PBMC) were collected from each individual as previously described (23).

RNA purification

Total RNA was extracted using a protocol adapted from Chomczynski and Sacchi using a pellet of 5×10^6 cells or 200 μl of plasma (24). RNA was resuspended in 30 μl of nuclease-free water. RNA concentrations were determined by spectrophotometry (GeneQuant, Pharmacia).

Plasmids

The HCV subgenomic replicon pFK-I$_{377}$neo/NS3-3′/wt (accession number: AJ242652) was kindly provided by Dr. R. Bartenschlager (University of Heidelberg, Germany) (22). Plasmid dl Δ-EMCV was kindly provided by Dr. P. Sarnow (Stanford University, USA) and corresponds to the Renilla luciferase-delta EMCV-Firefly luciferase vector that lacks an active IRES element (25,26). For the construction of vector DL-HCV 1b the HCV 1b IRES (nucleotide 13 to 383; AJ242652) was recovered by a one-step reverse transcription (RT)-polymerase-chain reaction (PCR) using the SuperScript^{TM} III one step RT-PCR system with Platinum$^{®}$ Taq DNA Polymerase (Invitrogen) kit from the HCV subgenomic replicon pFK-I$_{377}$neo/NS3-3′/wt using primers P1-XhoI (5′GCCGCTCGAGTTGGGGGGCGACACTCCACCAT AGATC 3′) and P4-EcoRI (5′ CGGGGAATTCGTTAC GTTTGGTTTTTCTTTGAGG 3′). The amplicon was cloned into the pGemT-easy vector (Promega). The pGemT plasmid DNA harboring the HCV 1b IRES was digested with XhoI and EcoRI and the recovered HCV IRES was cloned into the intercistronic region of the dual luciferase (DL) (RLuc/FLuc) vector described in Brasey *et al.* (25) previously digested with XhoI and EcoRI to eliminate the Δ-EMCV-HIV-1 IRES sequences. HCV IRESes were recovered from total RNA purified from clinical samples by a one step RT-PCR using the SuperScript^{TM} III one step RT-PCR system with Platinum$^{®}$ Taq DNA Polymerase (Invitrogen) kit using the P1-XhoI and P4-EcoRI primers and cloned directly into the pGemT-easy vector (Promega). pGemT plasmids harboring the HCV IRESes recovered from bacterial colonies were digested with XhoI and EcoRI and the viral IRES was cloned into the intercistronic region of the dual luciferase (DL) (RLuc/FLuc) as described above. All clones were sequenced (Macrogen Corp, USA) and aligned against the HCV prototype sequences using the
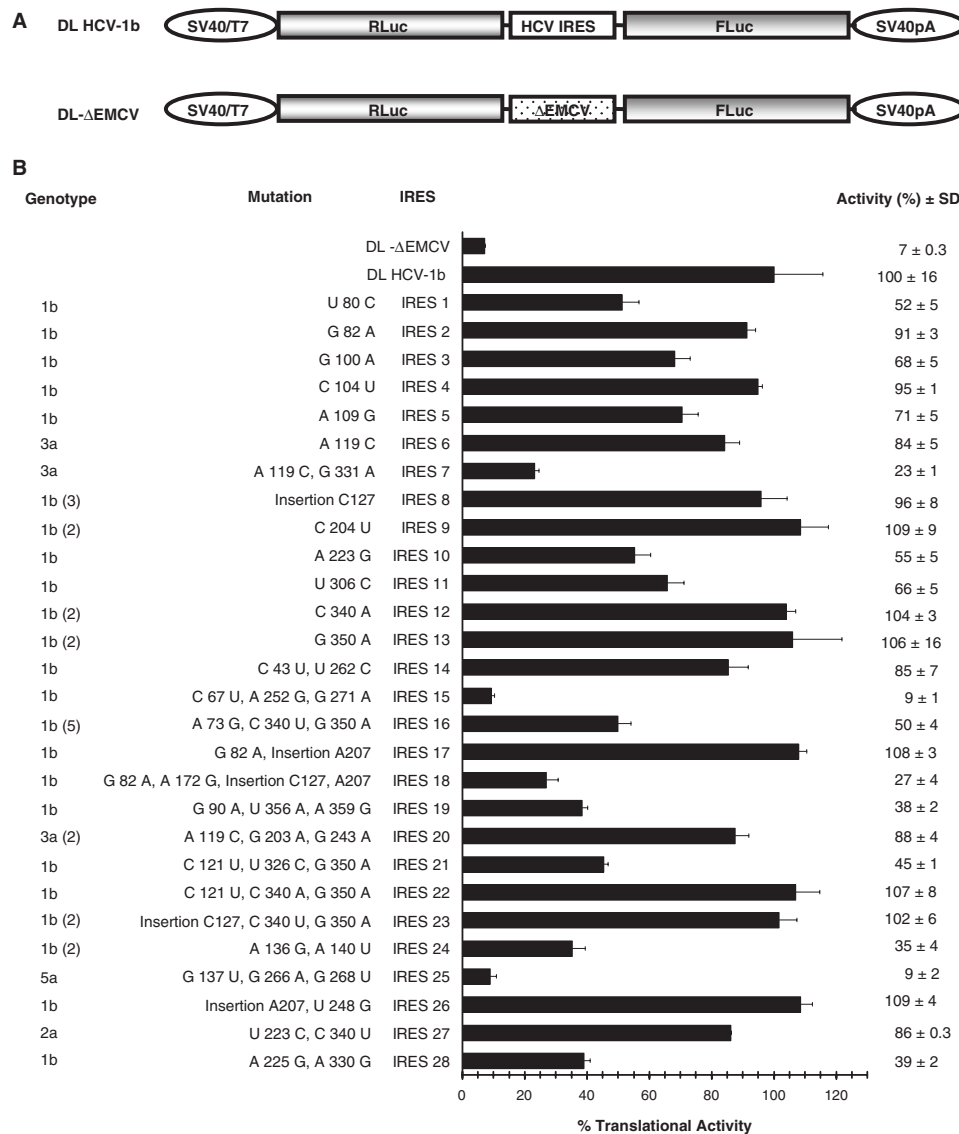
A

DL HCV-1b: SV40/T7 — RLuc — HCV IRES — FLuc — SV40pA

DL-ΔEMCV: SV40/T7 — RLuc — ΔEMCV — FLuc — SV40pA

B

Genotype	Mutation	IRES	Activity (%) ± SD
		DL -ΔEMCV	7 ± 0.3
		DL HCV-1b	100 ± 16
1b	U 80 C	IRES 1	52 ± 5
1b	G 82 A	IRES 2	91 ± 3
1b	G 100 A	IRES 3	68 ± 5
1b	C 104 U	IRES 4	95 ± 1
1b	A 109 G	IRES 5	71 ± 5
3a	A 119 C	IRES 6	84 ± 5
3a	A 119 C, G 331 A	IRES 7	23 ± 1
1b (3)	Insertion C127	IRES 8	96 ± 8
1b (2)	C 204 U	IRES 9	109 ± 9
1b	A 223 G	IRES 10	55 ± 5
1b	U 306 C	IRES 11	66 ± 5
1b (2)	C 340 A	IRES 12	104 ± 3
1b (2)	G 350 A	IRES 13	106 ± 16
1b	C 43 U, U 262 C	IRES 14	85 ± 7
1b	C 67 U, A 252 G, G 271 A	IRES 15	9 ± 1
1b (5)	A 73 G, C 340 U, G 350 A	IRES 16	50 ± 4
1b	G 82 A, Insertion A207	IRES 17	108 ± 3
1b	G 82 A, A 172 G, Insertion C127, A207	IRES 18	27 ± 4
1b	G 90 A, U 356 A, A 359 G	IRES 19	38 ± 2
3a (2)	A 119 C, G 203 A, G 243 A	IRES 20	88 ± 4
1b	C 121 U, U 326 C, G 350 A	IRES 21	45 ± 1
1b	C 121 U, C 340 A, G 350 A	IRES 22	107 ± 8
1b (2)	Insertion C127, C 340 U, G 350 A	IRES 23	102 ± 6
1b (2)	A 136 G, A 140 U	IRES 24	35 ± 4
5a	G 137 U, G 266 A, G 268 U	IRES 25	9 ± 2
1b	Insertion A207, U 248 G	IRES 26	109 ± 4
2a	U 223 C, C 340 U	IRES 27	86 ± 0.3
1b	A 225 G, A 330 G	IRES 28	39 ± 2

% Translational Activity (0, 20, 40, 60, 80, 100, 120)

Figure 1. Translational activity of the natural HCV IRES variant isolated from clinical samples. (**A**). Schematic representation of the bicistronic constructs used. The HCV IRESes recovered from clinical samples were cloned into dual Luciferase bicistronic (DL) vectors harboring Renilla (RLuc) and Firefly (FLuc) luciferases as reporter genes. The 1b HCV IRES recovered from the HCV subgenomic replicon pFK-I$_{377}$neo/NS3-3′/wt (22), was cloned into a DL-vector to generate plasmid DL HCV-1b, the positive control. The RLuc/FLuc bicistronic vector harboring a defective encephalomyocarditis virus (ΔEMCV) IRES, named DL-ΔEMCV, known to inhibit ribosome reinitiation and readthrough, inserted upstream of the FLuc reporter was used as a negative control (25,26). (**B**) HCV IRESes arbitrarily numbered 1–28 isolated from clinical samples were cloned into the DL-vector. Viral genotype and number of recovered clones, number in brackets, are shown. Natural variations within the IRES nucleotide sequence were identified by sequencing followed by alignment with the 5′UTR of HCV genotype 1b (AJ238799.1), 2a (D00944), 3a (D17763) and 5a (Y13184) prototypes. DL-vectors were arbitrarily named according to their IRES, from 1 to 28 (IRES 1–28). Translational activity of the different DL RNAs with HCV-IRESes 1–28 were evaluated in comparison with the DL HCV-1b and the DL-ΔEMCV control RNAs in the RRL. RLuc and FLuc activities were measured and the [(FLuc/RLuc)] ratio was used as an index of IRES activity. The [(FLuc/RLuc)] ratio of the DL IRES-1b RNA was arbitrarily set at 100%. Values are the means +/– SD from three independent experiments.

CLUSTAL W program (27). A schematic representation of the bicistronic vectors used in this study is shown in Figure 1A. For the generation of mutants C67T, A73G and G90A the DL-RLuc/FLuc vector harboring IRESes isolated from clinical samples containing each of the mutation were digested with XhoI and AgeI and ligated into the DL-RLuc/FLuc vector contained the HCV 1b IRES previously digested with XhoI and AgeI. For the generation of mutants A223G, U306C, C340T/G350A and U356A/A359G the DL-RLuc/FLuc vector harboring IRESes isolated from clinical samples containing the mutation were digested with AgeI and EcoRI and cloned into the DL-RLuc/FLuc vector contained the HCV 1b IRES previously digested with AgeI and EcoRI. For the construction of the HCV IRES G82A/A172G and A119C/G331A double mutants the DL-RLuc/FLuc vector contained mutation A172G and G331A, respectively, obtained by PCR (as described

Table 1. Oligonucleotides used to generate the mutant HCV 1b IRESes described in this study

Name	Orientation	Sequence (5′ to 3′)
renFw	Sense	TCGGACCCAGGATTCTTTTC
P2anti	Antisense	TCTCTTCATAGCCTTATGCAGTTG
P1tag	Sense	TGGCGAATAATTGGGGGCGACAC TCCACCATAG
mut1	Antisense	CGCCATGGtTAGACGCTTTC
mut2	Antisense	TCCCGGGAGGGGGGGGgCCT
mut3	Antisense	CACTATGGaTCTCCCGGGAG
mut4	Antisense	CGCCATGGtTAGACGCTTTC
mut5	Antisense	CTACTCGGCcAGCAGTCTCG
mut6	Antisense	TCGCGACCtAACACTACTCG
mut7	Antisense	TCGCGAaCCAACACTACTCG
mut8	Antisense	AAGGCCTTTCGtGACCCAAC
mut9	Antisense	TGCACGGTtTACGAGACCTG
mut10	Antisense	CTTTCGtGACCCAACACTACTCG GCcAGCAG
mut11	Antisense	TCGCGAaCtAACACTACTCG

Mutations introduced in the HCV IRES are in lower case and in bold.

below) were digested with AgeI and EcoRI and the fragment was ligated with the DL-RLuc/FLuc vector harboring the G82A and A119C changes, respectively, previously digested with AgeI and EcoRI. Point mutations G82A, A119C, G137T, A172G, A252G, G266A, G268T, G271A, G331A, A252G/G271A and G266A/G268T (primers mut 1 to 11, respectively) were introduced into the DL-RLuc/FLuc vector harboring the HCV 1b IRES following a PCR-based mutagenesis protocol (28), using three common oligonucleotides (renFw, P2anti and P1tag) and one mutation-specific oligonucleotide (mut 1-mut 11) for each mutant (Table 1). To obtain plasmids the DL-RLuc/FLuc vector harboring the mutant IRES two successive rounds of PCR using Platinum Taq DNA polymerase High Fidelity (Invitrogen) were conducted. The first round consists of two simultaneous PCR reactions one using the renFw and the different mut primers (containing the mutation, Table 1) while the second PCR was conducted using primers P1tag and P2anti (Table 1). Amplicons from each PCR reaction were purified, mixed and subjected to another round of PCR using the external primers renFw and P2anti (Table 1). The resulting PCR products were digested with XhoI and EcoRI and ligated into the intercistronic region of the DL-RLuc/FLuc vector previously digested with XhoI and EcoRI (see above). All constructs were verified by sequencing (Macrogen Corp, USA). Oligonucleotides used in this study are listed in Table 1.

In vitro transcription

Uncapped mRNAs were synthesized with T7 RNA polymerase (Fermentas). In brief, plasmids linearized with BamHI were used for *in vitro* transcription in a 25 μl final volume. The template DNA was digested with DNase I, and RNA was precipitated with 2.5 M LiCl. RNA was resuspended in diethyl pyrocarbonate (DEPC)-treated water. Capped mRNAs were synthesized using the mMESSAGE mMACHINE High Yield Capped RNA Transcription Kits (Ambion, Applied Biosystems)

following manufacturer's specifications. The poly(A) tailing kit (Ambion, Applied Biosystems) was used to add poly(A) tail to the capped mRNAs according to the manufacturer's specifications. RNA concentrations were determined spectrophotometrically and RNA integrity was monitored by electrophoresis on denaturing-agarose gels.

In vitro translation

For *in vitro* translations nuclease-treated rabbit reticulocyte lysate (35% RRL, Promega) were programmed with 8 ng/μl of RNA and reactions were performed at 90 min at 30°C, using salt conditions described in Svitkin *et al.* (29). Human hepatoma cell line, Huh-7 (kindly provided by Dr. Bartenschlager) were grown as previously described (22), and Huh-7 based cell free translation extracts that were prepared according to previously published protocols (29). Huh-7 translation extracts (50%) were programmed with 60 ng/μl of RNA and translation was conducted for 90 min at 30°C. Renilla and Firefly Luciferase activities were measured in a single tube using the Dual-Luciferase® Reporter Assay System (Promega) on a Sirius luminometer (Berthold Detection Systems) according to the manufacturer's protocol.

Tranfection of Huh-7 cell

The 5′capped and 3′polyadenylated bicistronic RNAs harboring the mutant IRESes were transfected into Huh-7 cells using Lipofectamine 2000 Transfection Reagent (Invitrogen) according to the manufacturer's protocol. Huh-7 cells were grown to 90% confluence in 12-well tissue culture plates and transfected with a total of 400 ng of capped/polyadenylated RNA. Cells were directly harvested with Passive Lysis 1X Buffer (Promega) 6–7 h post-transfection, and analyzed for luciferase as described above. The protein content of all samples was determined using the Bio-Rad Protein Assay (Bio-Rad Laboratories, Inc.).

HCV genotyping

HCV genotyping of virus present in plasma and PBMCs was performed using the reverse-hybridization line probe assay, INNO-LiPA HCV II kit (Innogenetics, Ghent, Belgium) according to the manufacturer's instructions. Genotyping was confirmed by sequencing (Macrogen Corp, USA) and phylogenetic analysis as previously described (23).

MD simulations

The HCV IRES IIId starting structure (wild type) was the best representative conformer of the experimental NMR data obtained by Lukavsky *et al.* (20; PDBid: 1F84). Mutants models (G266A, G268U and G266A/G268U) were generated from the wt structure using the Nucleic Acid Modeling tool within Discovery Studio® research environment (Discovery Studio v1.7. Accelrys Inc., San Diego 2007). Hydrogen atoms were energy minimized by CHARMM (30,31), until a convergence of 0.001 kcal/mol·Å. During the minimization, the heavy atoms were

held fixed and an implicit distance-dependent dielectric solvent model was employed (32). The wt and mutant models were embedded in a periodic box ($72 \times 96 \times 72$) containing $\sim$14 800 water molecules. The water phase was extended to a distance of 25 Å from every solute atom and the RNA helix charges were neutralized by addition of 29 Na^+ counterions. Molecular dynamics simulations were carried out using the NAMD v 2.6 program (33). Nucleic acids parameters were taken from the Cornell force field (34), combined with the TIP3P water model parameters from CHARMM27 (35). Initial structures were energy minimized by conjugate gradient algorithm until a gradient tolerance of 0.001 was reached. After minimization, system temperature was raised in 30 000 steps to 298 K (0.01 K by step) by temperature reassignment method followed by 1 ns of equilibration. During heating and equilibration, initial harmonic constraints on heavy atoms were gradually turned off in rounds of 500 ps to a final value of 0. Production runs were performed during 6 ns at integration step of 1 fs in the isothermic–isobaric thermodynamic ensemble at 298 K using the Settle algorithm on bonds involving water hydrogen atoms. Van der Waals interactions were truncated at 12 Å, while electrostatic interactions were fully calculated with the Particle Mesh Ewald (PME) method. Non-bonded and long-range electrostatics forces were evaluated every 2 and 4 fs, respectively.

Structural analysis

The calculation of the conformational space reachable by the individual nucleotides during the MD simulation was performed by the computation of the pseudotorsions angles between the two virtual bonds η ($C4'_{i-1}-P_i-C4'-P_{i+1}$) and θ ($P_i-C4'-P_{i+1}-C4'_{i+1}$) (36). Aromatic interactions between nucleotides were estimated by both; the distance between the centers of mass (COMs) of the aromatic bases, and by the α angle between the aromatic ring planes defined as the dot product of their normal vectors (37).

CD spectroscopy measurements

CD measurements were performed with a Jasco J-600 spectropolarimeter. Twenty-seven-nt RNAs corresponding to the HCV stem–loop IIId wt (nt 253–279, HCV 1b) or mutants G266A, G268U and G266A/G268U used in these assays were synthesized by Integrated DNA Technologies (Coralville, USA). Samples contained 11–16 μM RNA in water or 1, 2 or 5 mM $MgCl_2$ were analyzed in a 1 mm CD quartz cuvette. RNA denaturation/renaturation experiments were performed as previously described (38). Wavelength scans were recorded from 200 to 300 nm at 50 nm/min at 25°C, using a 1 nm bandwidth, a 1 s response time. All the CD spectra were corrected by subtraction of the background for the spectrum obtained with water or $MgCl_2$ at the appropriate concentration. Spectra were averaged over four to five accumulations. Results were expressed as mean residue ellipticity, in degrees $cm^2 dmol^{-1}$ (38).

RESULTS

Isolation of HCV-IRES variants from viruses from the plasma and PBMCs of HCV chronically infected patients

Fifty-four IRESes (nt 13–383) randomly isolated from clinical samples (plasma and PBMCs) obtained from 19 different HCV chronically infected individuals were cloned into a dual luciferase (DL) reporter construct containing an upstream *Renilla* luciferase gene (RLuc) and a downstream firefly luciferase gene (FLuc). In this context the HCV IRES activity was monitored using the FLuc activity as the readout, while the RLuc reporter gene serves as an upstream translational control (Figure 1A). The RLuc/FLuc bicistronic vector harboring the type 1b IRES of the HCV subgenomic replicon pFK-I$_{377}$neo/NS3-3′/wt (22) was used as a positive control, while a DL-vectors containing a defective encephalomyocarditis virus (Δ-EMCV) IRES (Figure 1A), known to inhibit ribosome reinitiation and readthrough, inserted upstream of the FLuc reporter was used as a negative control (25,26).

Sequencing of the 5′UTR followed by alignment analysis (data not shown) revealed that 89% of the isolated IRESes corresponded to genotype 1b, 7% to genotype 3a, 2% to genotype 2a and 2% to genotype 5a (Figure 1B). IRESes were considered natural variants if they presented at least one nucleotide difference when compared to the reference genotype. In this study, the sequences from genotype 1b (AJ238799.1), 2a (D00944), 3a (D17763) and 5a (Y13184) were used as reference sequences. Natural variations in the nucleotide sequence of the HCV 5′UTR are referred to from here on as mutations. Sequence alignments showed that 14 out of the 48 1b isolated IRESes were identical in sequence to the control HCV-1b IRES (data not shown). In some cases similar mutant IRESes (IRES 8, IRES 9, IRES 12, IRES 13, IRES16, IRES 20, IRES 23 and IRES 24 in Figure 1B) were isolated from different patients. In summary, only 28 of the initial 54 isolated IRESes, arbitrarily named 1–28, presented different sets of mutations when compared with the reference sequences (Figure 1B).

In vitro activity of the natural variants of the HCV-IRES isolated from clinical samples

Next we evaluated the ability of the HCV IRESes recovered from clinical samples to drive translation in the RRL (Figure 1B). The FLuc/RLuc ratio was used as an index of IRES activity, with the mean translation efficiency of the control HCV-1b IRES and the 14 1b-IRESes isolated from the clinical samples being arbitrarily set at 100% ($\pm$ SD). As shown in Figure 1B, the relative translation efficiencies (RTEs) of the variant IRESes differed considerably, from 9 to 109% when compared with the HCV-1b control. The residual activity of the DL-ΔEMCV RNA, lacking IRES activity, is 7% relative to the HCV-1b IRES. The RTE of the DL-ΔEMCV control vector was not subtracted from the RTE activities presented in Figure 1B. These observations are therefore in concordance with results reported in previous studies (19–21,39–43), and confirm that not all mutations impacted equally on HCV-IRES activity.

Influence of the mutations identified in natural IRES variants on the activity of the HCV-1b IRES

To determine the influence of each of the mutations on viral IRES activity, substitutions were introduced into the HCV-1b IRES and their effect on translation was evaluated *in vitro*. We focused our study on nucleotide changes found in mutant IRESes with an impaired RTE (Figure 1B). DL-vectors with the different mutant IRESes were named according to the nucleotide change with respect to the control HCV-1b IRES. The ability of the different mutants to drive translation in RRL was evaluated using the FLuc/RLuc ratio as an index of IRES activity, with the mean translation efficiency of the control HCV-1b IRES being arbitrarily set to 100%. Figure 2A summarizes our findings. Mutations present in subdomain IIId are excluded from this scrutiny as they are independently analyzed in the next section.

In general, mutations in domain II had a moderate effect on translation efficiency (RTE ranged from 95% to 52%; Figures 1B and 2A). Transition U80C, located in the apical loop, had the most dramatic effect on IRES activity (RTE value of 52%). This finding is supported by a previous report showing a similar level of translation inhibition for the U80C and the U80A mutants (44). Mutation of nucleotide C104, shown to participate in a noncanonical base pair at the interaction surface of the IRES with the 40S ribosomal subunit (45), or of nucleotide A109 located at a Mg^{2+} binding site required to stabilize the conformation of subdomain IIa (45), had only a marginal effect on HCV IRES activity with RTE values of 95% and 71%, respectively (Figure 1B).

Mutation G331A, predicted to destabilize a G331-C354 Watson–Crick interaction between the noncoding and coding portions of the viral IRES, in domain IV severely hindered HCV IRES translational activity (RTE of 28%; Figure 2A). Other mutations found in domain IV, such as C340A (RTE of 104%) and G350A (RTE of 106%) did not significantly alter IRES activity (Figure 1B). The natural variant A119C/G331A (IRES 7) had a RTE of 23% (Figure 1B). Both mutations, when simultaneously introduced into the 1b-IRES consistently resulted in a translational activity of 21% (Figure 2A). However, on its own the A119C transversion merely reduced 1b-IRES activity to 72% (Figure 2A), which is similar to the RTE of 84% observed for the natural variant IRES 6 (Figure 1B). Thus, we conclude that the G331A transition is responsible for the diminished IRES activity presented by IRES 7 (Figures 1B and 2A).

Activity of IRES 18 (G82A/A172G/C127 and A207 insertions) was decreased by 73% (Figure 1B). As insertion C127 (IRES 8; Figure 1B) had marginal effects on HCV IRES activity, and mutation G82A/A207 insertion had no effect on IRES activity (IRES 17, Figure 1B), we predicted that mutation A172G alone was responsible for the low translational activity exhibited by IRES 18 (Figure 1B). The A172G substitution is expected to disrupt the Watson–Crick A172-U227 pair in helix IIIb disturbing the network of bonds required for keeping the IIIabc junction together (19), disruption of which is expected to compromise the ability of the IRES to bind eIF3 and the ribosome (19). In agreement with this prediction overall translational activity was reduced to 30% when the A172G mutation was introduced in the context of the 1b-IRES (Figure 2A). The low translational activity (RTE of 32%) of IRES G82A/A172G further validates our conclusion (Figure 2A). Note that the A172G transition did not affect IRES activity as severely as the previously described A172U transvertion (19), suggesting that the conservation of a purine residue at position 172 might partially preserve the structure of the IIIabc junction.

HCV IRES activity is highly susceptible to mutations within subdomain IIId

HCV IRES subdomain IIId, which spans nucleotides 253 to 279, forms the most extensive contact of the HCV IRES on the 40S subunit body (20,46). Consistent with this function mutations or deletions in subdomain IIId are reported to be deleterious to HCV IRES activity (20,40–42,47). Consistent with these findings, results presented in Figure 1B show that IRESes 15 (C67U/A252G/G271A) and 25 (G137U/G266A/G268U), both harboring mutations within subdomain IIId, displayed RTEs equivalent to the DL-ΔEMCV vector. To establish if indeed the mutations present in subdomain IIId were responsible for the low RTE displayed by IRESes 15 and 25, each mutation was independently introduced into the 1b-IRES. Under these conditions mutations C67U and G137U had only limited effects on HCV IRES activity (RTE of 88% and 64%, respectively; Figure 2A). Therefore, on their own these mutations could not account for the lack of translational activity of IRESes 15 and 25. However, in agreement with previous reports (10,20,40–42), point mutations A252G, G266A, G268U and G271A (Figure 2B), diminished HCV IRES activity to 47%, 14%, 14% and 59%, respectively (Figure 2C). The dual substitution mutants A252G/G271A and G266A/G268U also showed important reductions in translational activity (RTE of 15% and 14%, respectively) (Figure 2C).

Biochemical reconstitution of the initiation process on the HCV IRES revealed that formation of the IRES-40S-eIF3 ternary preinitiation complex is independent of other eIFs (15). However, the HCV IRES requires cellular proteins for optimal translational activity (48,49). One plausible explanation for the impairment in translational activity observed for the different IIId mutants is that HCV IRES transacting factor(s) are absent from, or available in limiting concentrations in the RRL. To assess this possibility, translation efficiencies of the different IIId mutants were evaluated in Huh-7 cell-derived translation extracts (29). Huh-7 cells represent a well-characterized human hepatocellular carcinoma cell line known to support replication of the HCV subgenomic replicon and the JFH1 genotype 2a HCV strain (22,50). In Huh-7 cell-based translation extracts mutants A252G, G266A, G268U, G271A, A252G/G271A and G266A/G268U exhibited a drastic reduction in translational activity (Figure 2C). The apparent discrepancy between the results obtained in RRL (nuclease-treated) versus Huh-7 cell based translation extracts is likely due to the presence of
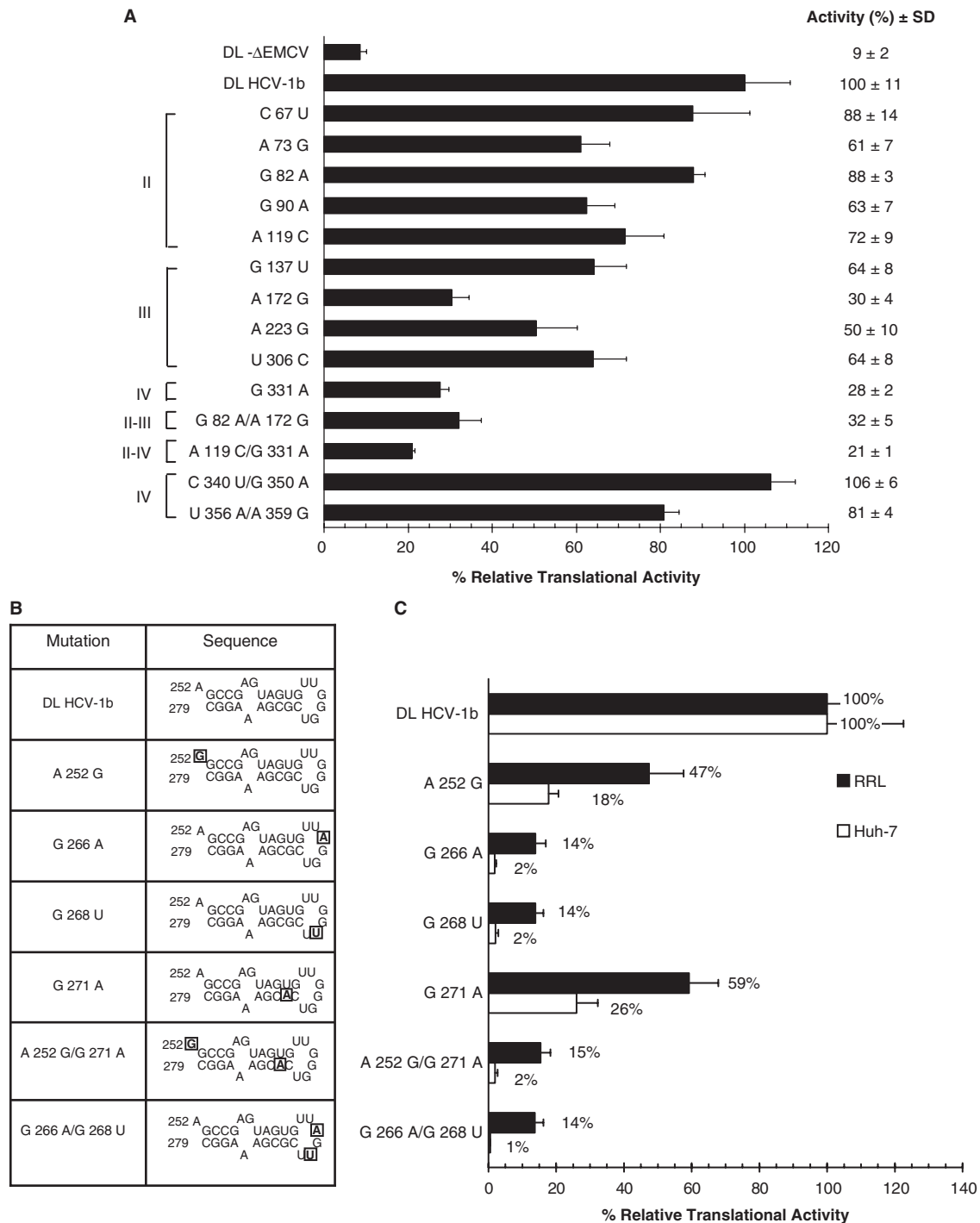
Figure 2. Mutational analysis of the HCV 1b IRES. (**A**) The ability of the different 1b IRES mutants, named according to the mutation, to drive translation in the RRL was monitored. In these assays the FLuc/RLuc ratio was used as an index of IRES activity, with the mean translation efficiency of DL HCV-1b RNA being arbitrarily set at 100%. The HCV domains that harbor the mutations are indicated. Values are mean ± SEM from three independent experiments. (**B**) Schematic depicting the secondary structure of the HCV IRES subdomain IIId showing the locations of the nucleotide mutations introduced into the HCV 1b IRES background. (**C**) The ability of the different 1b IRES mutants, named according to the mutation, to drive translation in the RRL (black bar) or in Huh-7 cell free translational extracts (white bars) programmed with *in vitro* synthesized RNA was monitored. In these assays the FLuc/RLuc ratio was used as an index of IRES activity, with the mean translation efficiency of DL HCV-1b RNA being arbitrarily set at 100%. Values are mean ± SEM from three independent experiments. (**D**) Capped and polyadenylated RNA corresponding to the DL-vectors harboring the wt- or the IRES mutants were transfected into Huh-7 cell lines. Expression of the first cistron, RLuc, used as an indicator of transfection efficiency, and the expression from the second cistron, FLuc are shown. The FLuc/RLuc ratio was used as an index of IRES activity, with the mean translation efficiency of DL HCV-1b RNA being arbitrarily set at 100%. Values are mean ± SD from three independent experiments.
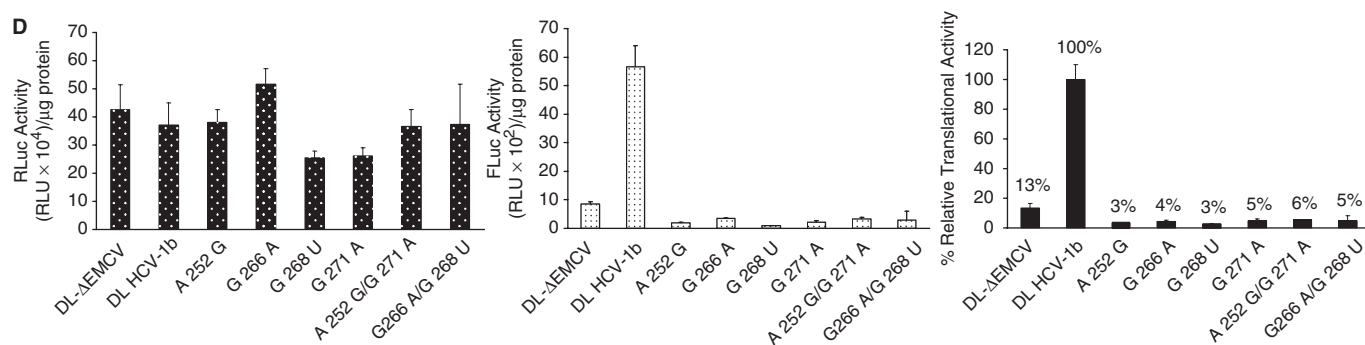
Figure 2. Continued.

endogenous mRNA in the latter, leading to competition for the translational apparatus and to lower translational activity.

To further challenge our observations we next assessed whether mutations within HCV IRES subdomain IIId reduce translation in cells. The rational for this experiment was derived from the report of Otto and Puglisi (6), who reported that deletion of the IIId loop-E motif diminished HCV IRES mediated translation in the RRL but not in cells. To this end, the *in vitro* generated, capped and poly-adenylated RNA corresponding to the DL-vectors harboring the wt- or the mutant-IRESes were transfected into Huh-7 cell lines (Figure 2D). Expression of the first cistron, RLuc, was used as an indicator of transfection efficiency (Figure 2D). Consistent with the data generated *in vitro*, mutations within subdomain IIId totally impaired HCV IRES activity in Huh-7 cells (Figure 2D).

MD simulations of HCV IRES subdomain IIId

The overall structure of subdomain IIId is well defined by NMR (20,51). Thus, to obtain insights into the molecular mechanisms by which mutations in the loop region of subdomain IIId might hinder HCV IRES activity, we used the NMR data to produce *in silico* models of HCV IRES wt and mutant IIId subdomain (Figure 3A). The dynamic behavior of these models was studied by means of MD simulations of the wt- and mutant-IIId subdomains, which exhibited a broad structural conservation of the average features that characterize the IIId domain (Figure 3A). Consistent with both the NMR data and previous MD simulation reports (20,52), the average root mean squared deviation (RMSD) values per nucleotide were <3 Å in all but the hexanucleotide (HN) hairpin loop region (Figure 3B). Strikingly, the MD simulations predicted that the G266A, G268U and G266A/G268U mutations only generate a local conformational change in the apical HN loop region (Figure 3A and B). When comparing the HN loop regions of the four MD models, mutant G268U appears to be the most disordered while the G266A/G268U double mutant exhibits higher stability (Figure 3A and B).

Some features within the HN loop region such as the base stacking between nucleotides 266 and 267, the location of nucleotide 268 above the major groove and the exposure of U269 to the solvent phase resulted in common elements to all the analyzed structures

(Figure 3D). The most noticeable difference between the four MD models is the conformational preference for nucleotide U265 (Figure 3B and C). NMR shows that in the wt-context U265 is highly disordered in comparison to the three guanosine residues (20). However, an analysis of pseudotorsion angles of the different MD models underscores the restricted conformation of U265 in the double mutant, highlighting clear differences between the single mutants and the wt model (Figure 3C) (36). These results further stress the higher stability of the G266A/G268U double mutant when compared to both the single mutants and to the wt-IIId MD models (Figure 3). Flexibility of U265 in the single mutants allows this nucleotide to locate toward the minor groove enabling the establishment of an aromatic stacking interaction with the nucleotide at position 266 (Figure 3D). This interaction, albeit observed only transiently during data collection (data not shown) is able to modify the local environment around nt 266 and 267, both important for IRES-40S subunit interaction (20). The increased stability in the HN hairpin region exhibited by the G266A/G268U double mutant can be explained by a noncanonical hydrogen bond interaction established between 2′-hydroxyl groups from nucleotides U264 and ribose U268 in the major groove of the structure (Figure 3D and E). This type of base–ribose interaction is known to stabilize RNA structures (53) and most probably restores, to some extent, the loop structure that is normally stabilized by a trans-wobble U264-G268 base pair (51). These data highlight the significance of the trans-wobble U264-G268 base pair in the structure conservation of subdomain IIId.

CD spectroscopy studies of the HCV IRES subdomain IIId

The MD data predicted that wt- and G266A/G268U mutant IIId folding was similar (Figure 3A). To challenge this prediction, we studied the circular dichroism spectra (CD) of a synthetic 27-nt RNA corresponding to the HCV IRES subdomain IIId (nt 253–279) (20). CD is mostly based on a comparative analysis between different structures, but provides essential information about the conformational properties of nucleic acids in solution (54). This experimental approach has previously been used to study the folding of the HCV IRES upon thermal melting (38). Controversy remains over the effect of Mg^{2+} ions on IRES structure (38,40,51), thus we first evaluated by CD the
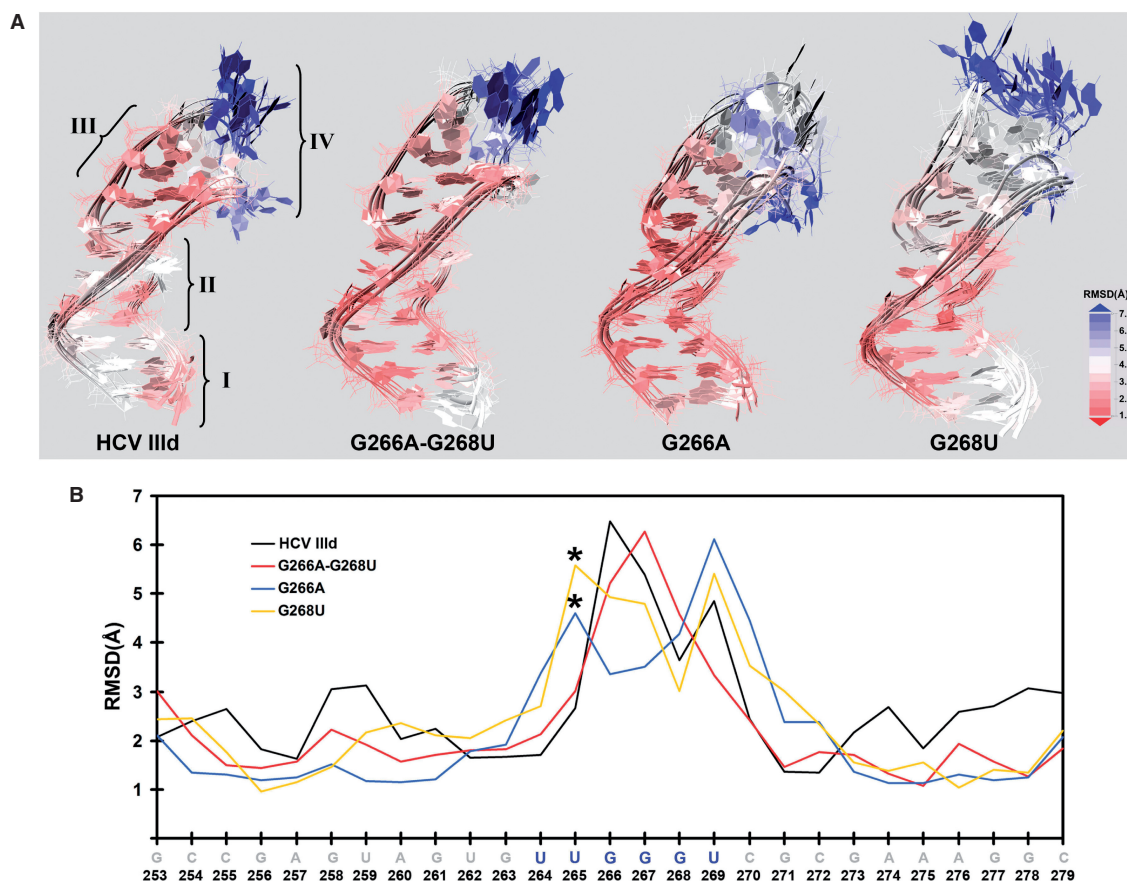
Figure 3. Structural study of HCV IRES subdomain IIId. (**A**) Comparative structural analysis of the subdomain IIId wild type and mutant models. Superimposed structures taken at 0, 1, 2, 3, 4, 5 and 6 ns of the collection phase of MD simulations. The structures are colored according to the average RMSD values. The main structural regions within subdomain IIId are mapped in the wild type model on left. Region I represents a right-handed A-form helix with Watson–Crick base pairing between nucleotides G253-C279, C254-G278 and C255-G277. Region II corresponds to a loop E structure with a characteristic S-turn composed of two sheared base pairs (G256-A276, A260-G273), a A257-A275 parallel base pair and a base triple between G258 and the reverse Hoogsteen pair U259-A274. Region III is an U262-G271 wobble base pair flanked by two Watson–Crick base pairs (G261-C272, G263-C270). Region IV is a disordered, -$_{264}$UUGGGU$_{269}$-, hexanucleotide (HN) loop region (20,51). (**B**) Average RMSD per nucleotide (computed for C3′ atoms) during 6 ns of MD simulation. In the *x*-axis the HN loop bases appear highlighted in blue. Average RMSD values for the U265 base in the single mutant models are highlighted with an asterisk. (**C**) η-θ plot of nucleotide U265 during the MD simulation of; I) the HCV wt-IIId; II) the G266A-G268U double mutant; III) the G266A mutant and IV) the G268U mutant presented according to (36). (**D**) A representative MD snapshot of the *in silico* generated models (see text) in which the base stacking among the apical HN nucleotides is presented. The aromatic rings of nucleotides 264 to 269 appear in tubular form (colored licorice) according to the atom types. The remaining nucleotides are represented by lines. The green arrowhead indicates the additional hydrogen bond recognized during the simulation. (**E**) Stability of intramolecular hydrogen bond in the double mutant G266A-G268U monitored during the MD experiment. Distances between the heavy atoms of the hydrogen donor and acceptor groups are plotted. This interaction, together with the Watson–Crick G263-U270 base pair contributes to a decrease in the mobility of residues in the HN loop region.

effect of Mg^{2+} ions (0, 1, 2 or 5 mM) on the folding of subdomain IIId upon thermal melting followed by rena-turation as previously described (38). The selection of ion concentrations was based on reports showing that a folding transition of the HCV IRES occurs at a 1 mM Mg^{2+} (40), *in vitro* HCV IRES activity is optimal at 2 mM Mg^{2+} (40,55) and HCV IRES is functional, albeit to a lesser extent, at 5 mM Mg^{2+} (38,56). Before conducting the assays we established the effect of Mg^{2+} ions on RNA aggregation. Consistent with previous reports (38,40), we found that all synthetic RNAs resolved as a sharp single band in native polyacrylamide gel electrophoresis in the presence of 0, 1, 2 or 5 mM Mg^{2+}, indicating an absence of RNA aggregation in these experimental conditions (data not shown).

The CD spectra of renatured wt-IIId RNA revealed that, in isolation, the renaturation of subdomain IIId (a synthetic 27-nt RNA) following thermal melting was ion-dependent (Figure 4A). The CD spectra of the wt-IIId and mutant-IIId RNAs exhibited two major peaks centered at 260 and 205 nm. These peaks are due to π–π electron transitions in the stacked planar bases, influenced by asymmetric 3′-endo sugar rings (38,54). The wavelengths of the peak are characteristic of RNA in an A-form helical conformation (38). Upon thermal melting the CD spectra of the wt-IIId significantly changed when RNA was rena-tured in presence of Mg^{2+} ions (Figure 4A). The change in the CD spectra are assumed to reflect the conformational change in the RNA induced by Mg^{2+} binding (38,54). The magnitude of peaks at 260 and 205 nm increased
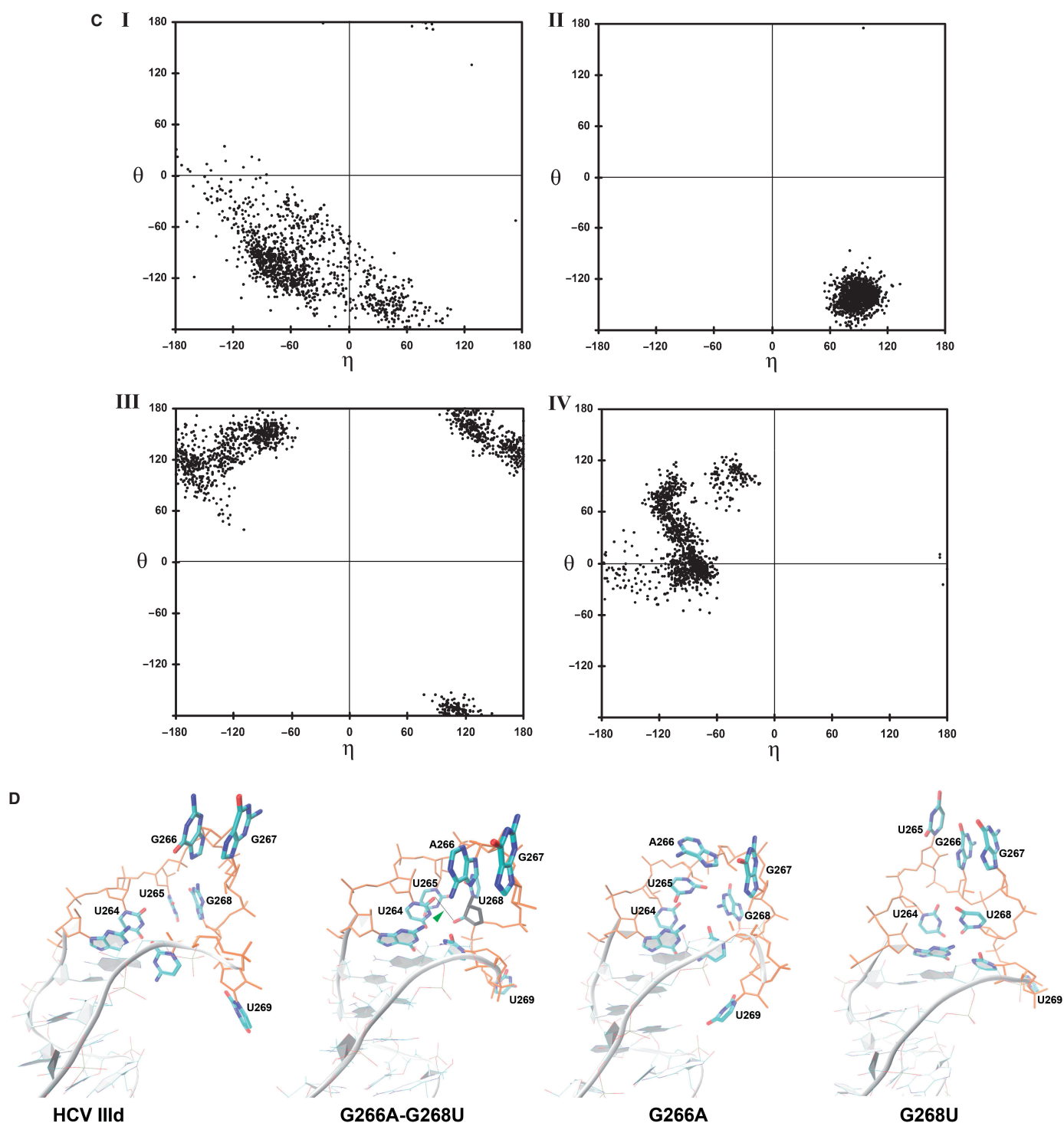
Figure 3. Continued.

when 1 and 2 mM MgCl$_2$ was added, indicating increased helix structure and base stacking. In agreement with previous reports a folding transition occurred between 0 and 1 mM Mg^{2+} (Figure 4A) (40). The structure of the subdomain IIId was maintained at 2 mM Mg^{2+}, while at 5 mM Mg^{2+} 260 and 205 nm peaks decreased relative to those at 1 and 2 mM Mg^{2+} (Figure 4A). Even though the effect of 5 mM Mg^{2+} on the conformational changes of

subdomain IIId cannot be readily explained, data were highly reproducible in repeat experiments. Taken together, these data stress that upon thermal denaturation Mg^{2+} ions are required to permit folding of subdomain IIId of the HCV IRES.

We next studied the CD renaturation spectra of the G266A, G268U and G266A/G268U mutant RNAs in the presence of 2 mM MgCl$_2$ and compared them to the

E
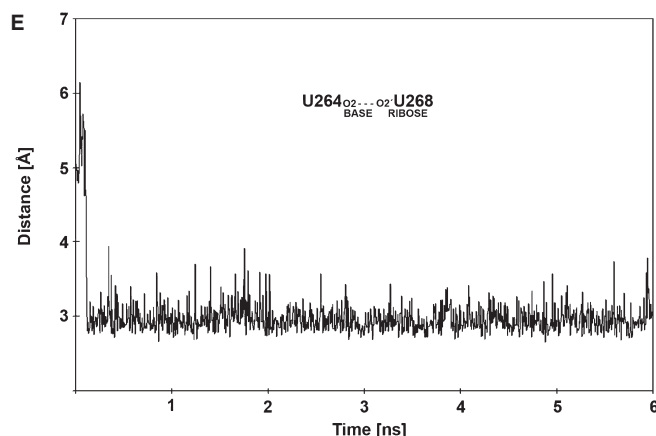
Figure 3. Continued.
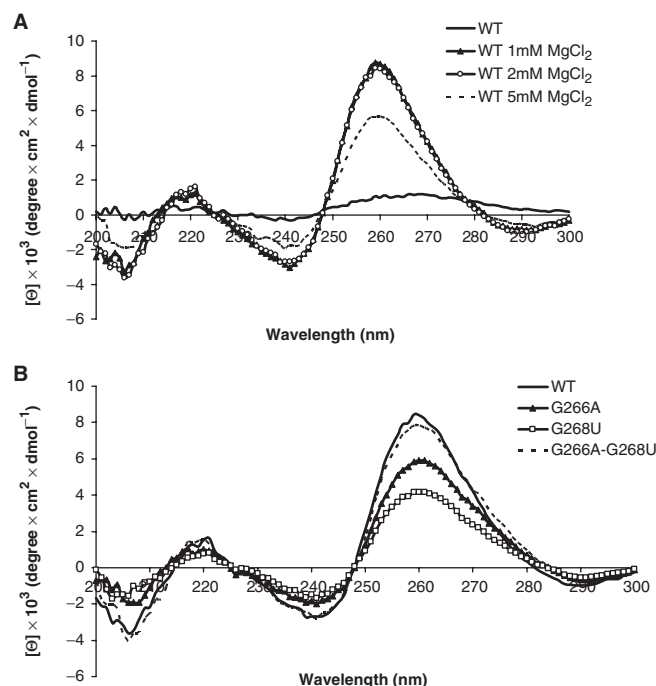
Figure 4. HCV IRES subdomain IIId adopts an ion-dependent structure. (**A**) Circular dichroism spectra (CD) of synthetic 27-nt RNAs corresponding to nucleotides 253–279 of the wt-IIId upon thermal melting followed by renaturation in the presence of in varying concentrations (0, 1, 2 and 5 mM) of MgCl$_2$. Wavelength scans were recorded from 200 to 300 nm as indicated in 'Materials and Methods' section. (**B**) CD of synthetic 27-nt RNA corresponding to nucleotides 253–279 of the wt and mutant IIId subdomains upon thermal melting followed by renaturation in the presence of 2 mM MgCl$_2$.

renaturation spectra of the wt-IIId RNA. Ion concentration affected the CD spectra of these RNAs in a dissimilar manner indicating, in the case of the native and the G266A/G268U double mutant RNAs, an increase in base stacking that might represent greater helix stability (Figure 4B). Moreover and consistent with the MD models (Figure 3), the CD spectra of the G266A/G268U double mutant strikingly resembled those of the wt-IIId,

yet both CD spectra clearly differed from those obtained for the G266A and G268U single mutants, suggesting dissimilar RNA structures. These observations are in agreement with previous reports showing that a G266C mutation alters the ion-dependent structure of the HCV IRES (40). Therefore, the structural differences between both single mutants and the wt-IIId domain may be responsible for the reduced IRES activity (Figure 2C).

Because the CD spectra obtained for the G266A/ G268U double mutant resembled those of the wt-IIId at 2 mM Mg^{2+} (Figure 4B) we decided to establish if this structural similarity was maintained at different Mg^{2+} concentrations (Figure 5). Noticeably, the double mutant and wt-IIId domains exhibited similar CD renaturation spectra in either the absence or the presence of different concentrations of Mg^{2+} ions indicating that, in isolation, the wt-IIId and G266A/G268U double mutant subdomain IIId share similar structural features (Figure 5). Overall, the evidence presented herein strongly suggests that mutations G266A/G268U hinder IRES activity without altering the structure of subdomain IIId.

DISCUSSION

The molecular mechanisms that determine the function of viral IRESes are not clearly understood. In the case of the HCV IRES the demonstration that many domain mutations resulting in reduced protein synthesis can be restored by compensatory mutations suggests that the IRES structure is required to initiate protein synthesis (9,13,19–21,57–59). Also, mutations in the loop regions of subdomains IIIc and IIIe indicate that the function of the HCV IRES relies, to some degree, on its primary sequence (39,60). In this study, we have sought to further understand the relation between IRES structure and function by analyzing natural variants of the HCV IRES isolated from clinical samples. Results of this study not only confirm the stringent structure/function relationship exhibited by the HCV IRES but also highlight the importance of the primary sequence of subdomain IIId in the translation of the viral mRNA.

Natural IRES variants of HCV genotypes 1b, 2a, 3a and 5a were isolated from clinical samples (Figure 1B). Sequencing analysis allowed the identification of naturally occurring mutations within the isolated IRESes (Figure 1B). Interestingly, a number of the variants identified herein have been previously found in clinical samples (39,41,61–63). The effect of the naturally occurring mutations on IRES-driven translation was evaluated by introducing each one in the wt-1b IRES background (Figures 1 and 2). Consistent with previous reports our results show that mutations within domains II and IV (Figures 1B and 2A) have a moderate effect on translation efficiency while mutations in domain III (Figure 2B–D) diminished the activity of the HCV IRES. Interestingly, among the natural IRES variants isolated in this study we identified mutations within subdomain IIId that hindered IRES activity without altering the local folding of this subdomain (Figures 2–5). To further understand how mutations within loop structures could diminish IRES
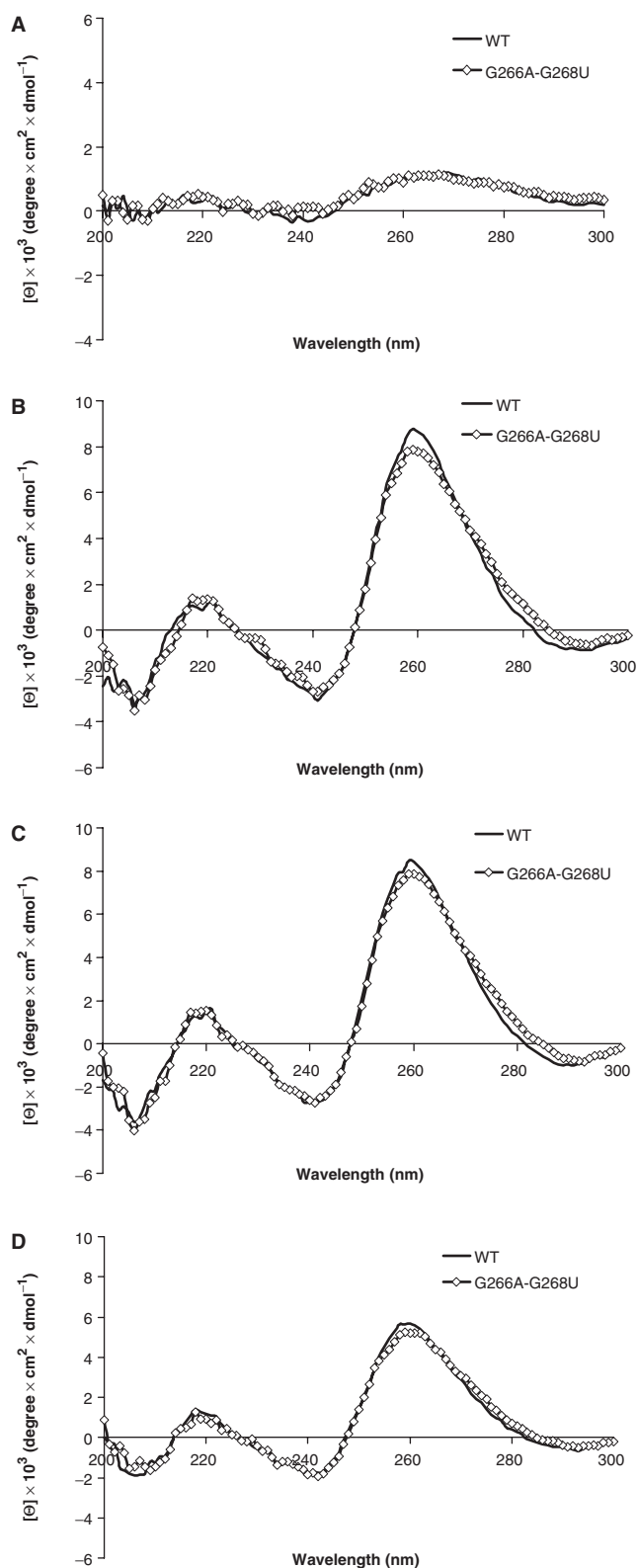
Figure 5. Wild-type and the G266A/G268U double mutant HCV IRES subdomain IIId adopt similar ion-dependent structures. CD of synthetic 27-nt RNA corresponding to nucleotides 253–279 of the wt or G266A/G268U double mutant-IIId upon thermal melting followed by renaturation in the presence of varying concentrations (**A**) 0, (**B**) 1 mM, (**C**) 2 mM and (**D**) 5 mM of MgCl$_2$.

activity we performed MD simulations on a model of the IIId domain developed on the basis of previously reported NMR data (20,51). Unexpectedly, MD simulations predicted that one of the tested IRES mutants, namely the G266A/G268U double mutant, shared similar structural features with the wt-IIId subdomain (Figure 3). This prediction was confirmed by CD spectrometry analysis at different Mg^{2+} ion concentrations (Figures 4 and 5). Together, these observations suggest that the G266A/G268U double mutant folded into a structure similar to the wt-IIId, yet the 1b-IRES that harbors these mutations lacks the ability to initiate translation. Consequently, it can be concluded that the primary sequence of subdomain IIId is required for optimal translation from the HCV IRES. Interestingly, the importance of the primary sequence in HCV IRES function does not seem to be restricted to the HN loop of subdomain IIId. A previous study describes that IRES activity is hindered by mutations within loops IIIc but that IRES folding is not altered (39). This sensitivity to primary sequence is not however a feature common to all loop structures within the HCV IRES. In agreement with previous reports (39,58,64) we describe insensitivity to mutational changes within the subdomain IIIb loop (IRES 9, Figure 1B), suggesting that in this case the primary sequence does not play a role in HCV IRES function.

Several models can be proposed to explain our observations. One possibility is that the primary sequence of the HN loop is important for preserving long distance RNA–RNA interactions of subdomain IIId with subdomains IIIe and IIIf (40), or between subdomain IIId and domain II (65). This option is consistent with data showing that subdomain IIId participates in IRES structural transitions affected by ions (38,40), and with observation indicating that mutations within this subdomain induce structural reorganization of the HCV IRES (42). Considering that subdomain IIId participates in the docking of the 40S ribosomal subunit, an alternative possibility is that mutations within this subdomain inhibit 40S ribosomal subunit binding to the IRES. In agreement with this option a previously described IRES mutant [G(266–268)C] exhibited reduced 40S binding affinity and resultant block of 48S preinitiation complex formation (8,10). However, our previous model fails to explain data generated using IRES mutant G(266–268)A (6,20). When compared to the wt-IRES the G(266–268)A mutant does not exhibit an altered secondary structure. The mutations only marginally alter the binding capacity of the 40S ribosomal subunit, yet, consistent with our findings nucleotide substitutions cause a severe translation defect (6,20). It would therefore seem that preserving the fold of subdomain IIId [G(266–268)A] is not sufficient to ensure IRES-activity (6,20).

After binding, the subsequent docking of the IRES ORF into the mRNA cleft requires some degree of structure melting. For example, nucleotide substitutions predicted to enhance the stability of the domain IV stem–loop are deleterious to translation initiation both *in vitro* and *in vivo* (18). Additional mutations that destabilize the stem–loop restored translation to a normal level (18). Thus, melting of some RNA domains may be required

for translation initiation to progress beyond 40S binding. The predicted stabilization of subdomain IIId in the G266A/G268U double mutant (Figure 3) may lock the 40S ribosomal subunit into a conformation which inhibits further steps of the initiation or the elongation process. Alternatively, stabilization of subdomain IIId may prevent the correct positioning of the 40S ribosomal subunit over the IRES element (6,66). This is of special relevance considering that correct binding of the 40S ribosomal subunit is required for the IRES to position the viral mRNA in the ribosomal P site without the assistance of canonical initiation factors.

In conclusion, the presented mutational and structural studies indicate that full functionality of the HCV IRES relies on both its primary sequence and secondary structure. Based on the stringent relationship between sequence/structure/function of subdomain IIId and on the fact that it is highly conserved among HCV genotypes it seems reasonable to propose that this subdomain of the HCV IRES holds promise as a specific target for the development of novel antiviral strategies directed against viral protein synthesis.

REFERENCES

1. Pestova,T.V., Kolupaeva,V.G., Lomakin,I.B., Pilipenko,E.V., Shatsky,I.N., Agol,V.I. and Hellen,C.U. (2001) Molecular mechanisms of translation initiation in eukaryotes. *Proc. Natl Acad. Sci. USA*, **98**, 7029–7036.
2. Lopez-Lastra,M., Rivas,A. and Barria,M.I. (2005) Protein synthesis in eukaryotes: the growing biological relevance of cap-independent translation initiation. *Biol. Res.*, **38**, 121–146.
3. Pestova,T.V., Lomakin,I.B., Lee,J.H., Choi,S.K., Dever,T.E. and Hellen,C.U. (2000) The joining of ribosomal subunits in eukaryotes requires eIF5B. *Nature*, **403**, 332–335.
4. Unbehaun,A., Borukhov,S.I., Hellen,C.U. and Pestova,T.V. (2004) Release of initiation factors from 48S complexes during ribosomal subunit joining and the link between establishment of codon-anticodon base-pairing and hydrolysis of eIF2-bound GTP. *Genes Dev.*, **18**, 3078–3093.
5. Pestova,T.V., Shatsky,I.N., Fletcher,S.P., Jackson,R.J. and Hellen,C.U. (1998) A prokaryotic-like mode of cytoplasmic eukaryotic ribosome binding to the initiation codon during internal translation initiation of hepatitis C and classical swine fever virus RNAs. *Genes Dev.*, **12**, 67–83.
6. Otto,G.A. and Puglisi,J.D. (2004) The pathway of HCV IRES-mediated translation initiation. *Cell*, **119**, 369–380.
7. Spahn,C.M., Kieft,J.S., Grassucci,R.A., Penczek,P.A., Zhou,K., Doudna,J.A. and Frank,J. (2001) Hepatitis C virus IRES RNA-induced changes in the conformation of the 40s ribosomal subunit. *Science*, **291**, 1959–1962.
8. Ji,H., Fraser,C.S., Yu,Y., Leary,J. and Doudna,J.A. (2004) Coordinated assembly of human translation initiation complexes by the hepatitis C virus internal ribosome entry site RNA. *Proc. Natl Acad. Sci. USA*, **101**, 16990–16995.
9. Reynolds,J.E., Kaminski,A., Carroll,A.R., Clarke,B.E., Rowlands,D.J. and Jackson,R.J. (1996) Internal initiation of translation of hepatitis C virus RNA: the ribosome entry site is at the authentic initiation codon. *RNA*, **2**, 867–878.
10. Kieft,J.S., Zhou,K., Jubin,R. and Doudna,J.A. (2001) Mechanism of ribosome recruitment by hepatitis C IRES RNA. *RNA*, **7**, 194–206.
11. Reynolds,J.E., Kaminski,A., Kettinen,H.J., Grace,K., Clarke,B.E., Carroll,A.R., Rowlands,D.J. and Jackson,R.J. (1995) Unique features of internal initiation of hepatitis C virus RNA translation. *EMBO J.*, **14**, 6010–6020.
12. Tsukiyama-Kohara,K., Iizuka,N., Kohara,M. and Nomoto,A. (1992) Internal ribosome entry site within hepatitis C virus RNA. *J. Virol.*, **66**, 1476–1483.
13. Honda,M., Ping,L.H., Rijnbrand,R.C., Amphlett,E., Clarke,B., Rowlands,D. and Lemon,S.M. (1996) Structural requirements for initiation of translation by internal ribosome entry within genome-length hepatitis C virus RNA. *Virology*, **222**, 31–42.
14. Fraser,C.S. and Doudna,J.A. (2007) Structural and mechanistic insights into hepatitis C viral translation initiation. *Nat. Rev. Microbiol.*, **5**, 29–38.
15. Sizova,D.V., Kolupaeva,V.G., Pestova,T.V., Shatsky,I.N. and Hellen,C.U. (1998) Specific interaction of eukaryotic translation initiation factor 3 with the 5' nontranslated regions of hepatitis C virus and classical swine fever virus RNAs. *J. Virol.*, **72**, 4775–4782.
16. Buratti,E., Tisminetzky,S., Zotti,M. and Baralle,F.E. (1998) Functional analysis of the interaction between HCV 5'UTR and putative subunits of eukaryotic translation initiation factor eIF3. *Nucleic Acids Res.*, **26**, 3179–3187.
17. Locker,N., Easton,L.E. and Lukavsky,P.J. (2007) HCV and CSFV IRES domain II mediate eIF2 release during 80S ribosome assembly. *EMBO J.*, **26**, 795–805.
18. Honda,M., Brown,E.A. and Lemon,S.M. (1996) Stability of a stem-loop involving the initiator AUG controls the efficiency of internal initiation of translation on hepatitis C virus RNA. *RNA*, **2**, 955–968.
19. Kieft,J.S., Zhou,K., Grech,A., Jubin,R. and Doudna,J.A. (2002) Crystal structure of an RNA tertiary domain essential to HCV IRES-mediated translation initiation. *Nat. Struct. Biol.*, **9**, 370–374.
20. Lukavsky,P.J., Otto,G.A., Lancaster,A.M., Sarnow,P. and Puglisi,J.D. (2000) Structures of two RNA domains essential for

hepatitis C virus internal ribosome entry site function. *Nat. Struct. Biol.*, **7**, 1105–1110.

21. Collier,A.J., Gallego,J., Klinck,R., Cole,P.T., Harris,S.J., Harrison,G.P., Aboul-Ela,F., Varani,G. and Walker,S. (2002) A conserved RNA structure within the HCV IRES eIF3-binding site. *Nat. Struct. Biol.*, **9**, 375–380.

22. Lohmann,V., Korner,F., Koch,J., Herian,U., Theilmann,L. and Bartenschlager,R. (1999) Replication of subgenomic hepatitis C virus RNAs in a hepatoma cell line. *Science*, **285**, 110–113.

23. Barria,M.I., Vera-Otarola,J., Leon,U., Vollrath,V., Marsac,D., Riquelme,A., Lopez-Lastra,M. and Soza,A. (2008) Influence of extrahepatic viral infection on the natural history of hepatitis C. *Ann. Hepatol.*, **7**, 136–143.

24. Chomczynski,P. and Sacchi,N. (1987) Single-step method of RNA isolation by acid guanidinium thiocyanate-phenol-chloroform extraction. *Anal. Biochem.*, **162**, 156–159.

25. Brasey,A., Lopez-Lastra,M., Ohlmann,T., Beerens,N., Berkhout,B., Darlix,J.L. and Sonenberg,N. (2003) The leader of human immunodeficiency virus type 1 genomic RNA harbors an internal ribosome entry segment that is active during the G2/M phase of the cell cycle. *J. Virol.*, **77**, 3939–3949.

26. Wilson,J.E., Powell,M.J., Hoover,S.E. and Sarnow,P. (2000) Naturally occurring dicistronic cricket paralysis virus RNA is regulated by two internal ribosome entry sites. *Mol. Cell. Biol.*, **20**, 4990–4999.

27. Thompson,J.D., Higgins,D.G. and Gibson,T.J. (1994) CLUSTAL W: improving the sensitivity of progressive multiple sequence alignment through sequence weighting, position-specific gap penalties and weight matrix choice. *Nucleic Acids Res.*, **22**, 4673–4680.

28. Mikaelian,I. and Sergeant,A. (1992) A general and fast method to generate multiple site directed mutations. *Nucleic Acids Res.*, **20**, 376.

29. Svitkin,Y.V., Pause,A., Lopez-Lastra,M., Perreault,S. and Sonenberg,N. (2005) Complete translation of the hepatitis C virus genome in vitro: membranes play a critical role in the maturation of all virus proteins except for NS3. *J. Virol.*, **79**, 6868–6881.

30. Brooks,B.R., Bruccoleri,R.E., Olafson,B.D., States,D.J., Swaminathan,S. and Karplus,M. (1983) CHARMM: a program for macromolecular energy minimization and dynamics calculations. *J. Comp. Chem.*, **00**, 187–217.

31. Momany,F.A. and Rone,R. (1992) Validation of the General Purpose QUANTA3.2/CHARMm Force Field. *J. Computat. Chem.*, **13**, 888–900.

32. Mazur,J. and Jernigan,R.L. (1991) Distance-dependent dielectric constants and their application to double-helical DNA. *Biopolymers*, **31**, 1615–1629.

33. Phillips,J.C., Braun,R., Wang,W., Gumbart,J., Tajkhorshid,E., Villa,E., Chipot,C., Skeel,R.D., Kale,L. and Schulten,K. (2005) Scalable molecular dynamics with NAMD. *J. Comput. Chem.*, **26**, 1781–1802.

34. Cornell,W.D., Cieplak,P., Bayley,C.I., Gould,I.R., Merz,K.M., Ferguson,D.M., Spellmeyer,D.C., Fox,T., Caldwell,J.W. and Kollman,P.A. (1995) A second generation force field for simulation of proteins, nucleic acids and organic molecules. *J. Am. Chem. Soc*, **117**, 5179–5197.

35. Foloppe,N. and MacKerell,A.D. (2000) All-atom empirical force field for nucleic acids: 2) parameter optimization based on small molecule and condensed phase macromolecular target data. *J. Comp. Chem.*, **21**, 86–104.

36. Duarte,C.M. and Pyle,A.M. (1998) Stepping through an RNA structure: a novel approach to conformational analysis. *J. Mol. Biol.*, **284**, 1465–1478.

37. Hunter,C.A., Singh,J. and Thornton,J.M. (1991) Pi-pi interactions: the geometry and energetics of phenylalanine-phenylalanine interactions in proteins. *J. Mol. Biol.*, **218**, 837–846.

38. Vos,S., Berrisford,D.J. and Avis,J.M. (2002) Effect of magnesium ions on the tertiary structure of the hepatitis C virus IRES and its affinity for the cyclic peptide antibiotic viomycin. *Biochemistry*, **41**, 5383–5396.

39. Tang,S., Collier,A.J. and Elliott,R.M. (1999) Alterations to both the primary and predicted secondary structure of stem-loop IIIc of the hepatitis C virus 1b 5' untranslated region (5'UTR) lead to mutants severely defective in translation which cannot be complemented in trans by the wild-type 5'UTR sequence. *J. Virol.*, **73**, 2359–2364.

40. Kieft,J.S., Zhou,K., Jubin,R., Murray,M.G., Lau,J.Y. and Doudna,J.A. (1999) The hepatitis C virus internal ribosome entry site adopts an ion-dependent tertiary fold. *J. Mol. Biol.*, **292**, 513–529.

41. Laporte,J., Malet,I., Andrieu,T., Thibault,V., Toulme,J.J., Wychowski,C., Pawlotsky,J.M., Huraux,J.M., Agut,H. and Cahour,A. (2000) Comparative analysis of translation efficiencies of hepatitis C virus 5' untranslated regions among intraindividual quasispecies present in chronic infection: opposite behaviors depending on cell type. *J. Virol.*, **74**, 10827–10833.

42. Jubin,R., Vantuno,N.E., Kieft,J.S., Murray,M.G., Doudna,J.A., Lau,J.Y. and Baroudy,B.M. (2000) Hepatitis C virus internal ribosome entry site (IRES) stem loop IIId contains a phylogenetically conserved GGG triplet essential for translation and IRES folding. *J. Virol.*, **74**, 10430–10437.

43. Odreman-Macchioli,F., Baralle,F.E. and Buratti,E. (2001) Mutational analysis of the different bulge regions of hepatitis C virus domain II and their influence on internal ribosome entry site translational ability. *J. Biol. Chem.*, **276**, 41648–41655.

44. Kalliampakou,K.I., Psaridi-Linardaki,L. and Mavromara,P. (2002) Mutational analysis of the apical region of domain II of the HCV IRES. *FEBS Lett.*, **511**, 79–84.

45. Lukavsky,P.J., Kim,I., Otto,G.A. and Puglisi,J.D. (2003) Structure of HCV IRES domain II determined by NMR. *Nat. Struct. Biol.*, **10**, 1033–1038.

46. Kolupaeva,V.G., Pestova,T.V. and Hellen,C.U. (2000) An enzymatic footprinting analysis of the interaction of 40S ribosomal subunits with the internal ribosomal entry site of hepatitis C virus. *J. Virol.*, **74**, 6242–6250.

47. Odreman-Macchioli,F.E., Tisminetzky,S.G., Zotti,M., Baralle,F.E. and Buratti,E. (2000) Influence of correct secondary and tertiary RNA folding on the binding of cellular factors to the HCV IRES. *Nucleic Acids Res.*, **28**, 875–885.

48. Costa-Mattioli,M., Svitkin,Y. and Sonenberg,N. (2004) La autoantigen is necessary for optimal function of the poliovirus and hepatitis C virus internal ribosome entry site in vivo and in vitro. *Mol. Cell Biol.*, **24**, 6861–6870.

49. Kim,J.H., Paek,K.Y., Ha,S.H., Cho,S., Choi,K., Kim,C.S., Ryu,S.H. and Jang,S.K. (2004) A cellular RNA-binding protein enhances internal ribosomal entry site-dependent translation through an interaction downstream of the hepatitis C virus polyprotein initiation codon. *Mol. Cell Biol.*, **24**, 7878–7890.

50. Wakita,T., Pietschmann,T., Kato,T., Date,T., Miyamoto,M., Zhao,Z., Murthy,K., Habermann,A., Krausslich,H.G., Mizokami,M. *et al.* (2005) Production of infectious hepatitis C virus in tissue culture from a cloned viral genome. *Nat. Med.*, **11**, 791–796.

51. Klinck,R., Westhof,E., Walker,S., Afshar,M., Collier,A. and Aboul-Ela,F. (2000) A potential RNA drug target in the hepatitis C virus internal ribosomal entry site. *RNA*, **6**, 1423–1431.

52. Golebiowski,J., Antonczak,S., Di-Giorgio,A., Condom,R. and Cabrol-Bass,D. (2004) Molecular dynamics simulation of hepatitis C virus IRES IIId domain: structural behavior, electrostatic and energetic analysis. *J. Mol. Model*, **10**, 60–68.

53. Tamura,M. and Holbrook,S.R. (2002) Sequence and structural conservation in RNA ribose zippers. *J. Mol. Biol.*, **320**, 455–474.

54. Sosnick,T.R., Fang,X. and Shelton,V.M. (2000) Application of circular dichroism to study RNA folding transitions. *Methods Enzymol.*, **317**, 393–409.

55. Borman,A.M., Bailly,J.L., Girard,M. and Kean,K.M. (1995) Picornavirus internal ribosome entry segments: comparison of translation efficiency and the requirements for optimal internal initiation of translation in vitro. *Nucleic Acids Res.*, **23**, 3656–3663.

56. Lancaster,A.M., Jan,E. and Sarnow,P. (2006) Initiation factor-independent translation mediated by the hepatitis C virus internal ribosome entry site. *RNA*, **12**, 894–902.

57. Rijnbrand,R., Bredenbeek,P., van der Straaten,T., Whetter,L., Inchauspe,G., Lemon,S. and Spaan,W. (1995) Almost the entire 5' non-translated region of hepatitis C virus is required for cap-independent translation. *FEBS Lett.*, **365**, 115–119.

58. Wang,C., Sarnow,P. and Siddiqui,A. (1994) A conserved helical element is essential for internal initiation of translation of hepatitis C virus RNA. *J. Virol.*, **68**, 7301–7307.

59. Varaklioti,A., Georgopoulou,U., Kakkanas,A., Psaridi,L., Serwe,M., Caselmann,W.H. and Mavromara,P. (1998) Mutational

analysis of two unstructured domains of the 5′ untranslated region of HCV RNA. *Biochem. Biophys. Res. Commun.*, **253**, 678–685.

60. Psaridi,L., Georgopoulou,U., Varaklioti,A. and Mavromara,P. (1999) Mutational analysis of a conserved tetraloop in the 5′ untranslated region of hepatitis C virus identifies a novel RNA element essential for the internal ribosome entry site function. *FEBS Lett.*, **453**, 49–53.

61. Forton,D.M., Karayiannis,P., Mahmud,N., Taylor-Robinson,S.D. and Thomas,H.C. (2004) Identification of unique hepatitis C virus quasispecies in the central nervous system and comparative analysis of internal translational efficiency of brain, liver, and serum variants. *J. Virol.*, **78**, 5170–5183.

62. Thelu,M.A., Drouet,E., Hilleret,M.N. and Zarski,J.P. (2004) Lack of clinical significance of variability in the internal ribosome entry site of hepatitis C virus. *J. Med. Virol.*, **72**, 396–405.

63. Motazakker,M., Preikschat,P., Elliott,J., Smith,C.A., Mills,P.R., Oien,K., Spence,E., Elliott,R.M. and McCruden,E.A. (2007) Translation efficiencies of the 5′-untranslated region of genotypes 1a and 3a in hepatitis C infected patients. *J. Med. Virol.*, **79**, 259–269.

64. Buratti,E., Gerotto,M., Pontisso,P., Alberti,A., Tisminetzky,S.G. and Baralle,F.E. (1997) In vivo translational efficiency of different hepatitis C virus 5′-UTRs. *FEBS Lett.*, **411**, 275–280.

65. Lafuente,E., Ramos,R. and Martinez-Salas,E. (2002) Long-range RNA-RNA interactions between distant regions of the hepatitis C virus internal ribosome entry site element. *J. Gen. Virol.*, **83**, 1113–1121.

66. Boehringer,D., Thermann,R., Ostareck-Lederer,A., Lewis,J.D. and Stark,H. (2005) Structure of the hepatitis C Virus IRES bound to the human 80S ribosome: remodeling of the HCV IRES. *Structure*, **13**, 1695–1706.